

# Exploring new physics in events with $E_T^{\text{miss}}$ and a Higgs boson decaying to two photons with the ATLAS detector

S. Liao, S. von Buddenbrock, D. Kar, B. Mellado, R. Reed, X. Ruan, K. Tomiwa

School of Physics, University of the Witwatersrand, 1 Jan Smuts Avenue, Braamfontein, Johannesburg, 2000, South Africa

E-mail: shell-may.liao@cern.ch

**Abstract.** The results of a search for new phenomena in events with missing transverse energy ( $E_T^{\text{miss}}$ ) and a Higgs boson decaying to two photons are presented. Data from proton-proton collisions at a centre-of-mass energy of 13 TeV, corresponding to an integrated luminosity of  $36.1 \text{ fb}^{-1}$  has been collected with the ATLAS detector at the LHC in 2015 and 2016. The results of this search are interpreted in terms of a model in which a heavy scalar, denoted ‘H’, decays into the Higgs boson and dark matter candidates ( $H \rightarrow h\chi\chi$ ). A model formulated based on inconsistencies in the Higgs boson transverse momentum distribution ( $p_{T,H}$ ) measured by ATLAS and CMS as well as other excesses in the data. Limits were placed on the branching ratio of  $H \rightarrow h\chi\chi$  using Run II data and the analysis is performed in several categories based on  $E_T^{\text{miss}}$  and  $E_T^{\text{miss}}$  significance ( $S_{E_T^{\text{miss}}}$ ) and splitting into the same vertex method. The results from this search are discussed.

## 1. Introduction

The discovery of the Higgs boson of  $m_H = 125 \text{ GeV}$  back in 2012 was one of the greatest achievements of the Large Hadron Collider (LHC) program at CERN [1, 2]. This discovery opened up new possibilities for physics beyond the Standard Model (BSM). The existence of dark matter (DM) particles is undeniably evident in astrophysics [3], but DM particles produced in SM collisions have a very small interaction probability. As a result, DM searches at the LHC are driven primarily by  $E_T^{\text{miss}}$  signatures produced with detectable particles ( $X + E_T^{\text{miss}}$ ). Both ATLAS and CMS have searched for topologies whereby the Standard Model (SM) Higgs boson is expected to be produced from a new interaction between DM and SM particles [4, 5]. This study presents an updated search for DM particles ( $\chi$ ) in association with the SM Higgs boson (h) decaying to a pair of photons using data collected at  $\sqrt{s} = 13 \text{ TeV}$  during 2015 and 2016.

There are three models considered in this search for DM [6] shown in figure 1. The  $Z'_B$  model [7] where a massive vector mediator emits a Higgs boson and decays into a pair of DM candidates. The  $Z'$ -2HDM model [7] whereby  $Z'$  is produced resonantly and decays into Higgs boson and an intermediate heavy pseudoscalar  $A^0$  which in turn decays into a pair of DM candidates. Finally, the heavy-scalar model [8] whereby a heavy-scalar boson (H) produced primarily via gluon-gluon fusion (ggF) with a mass in the range  $2m_h < m_H < 2m_{\text{top}}$  is introduced.

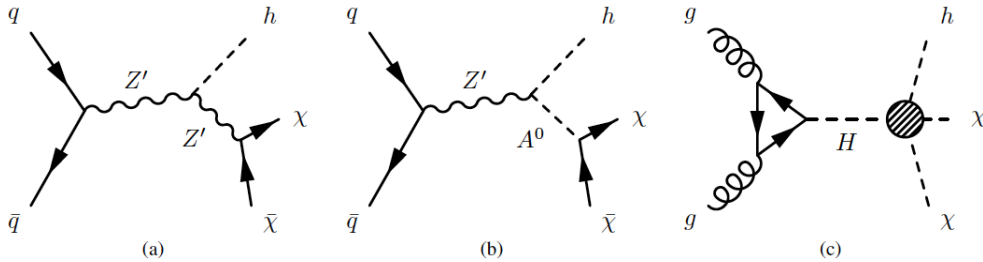


**Figure 1:** Feynman diagrams for the production of DM ( $\chi$ ) in association with a SM Higgs boson ( $h$ ) arising from three theoretical models considered in this analysis: (a)  $Z'_B$  model, (b)  $Z'$ -2HDM model, (c) heavy-scalar model.

This paper mainly discusses results from this heavy-scalar model. In this model, the upper bound on  $m_H$  is set in order to avoid a large branching fraction for  $H \rightarrow t\bar{t}$  which would lead to a  $H \rightarrow h\chi\chi$  branching fraction close to zero. The lower bound on  $m_H$  is set in order to ensure that the SM Higgs boson is produced on-shell. For simplicity, the decay branching fraction of  $H \rightarrow h\chi\chi$  is assumed to be 100% for this model and  $H$  can be viewed as being part of a 2HDM+ $\chi$  structure, where it may be considered as a CP-even heavy-scalar boson [8].

## 2. The ATLAS detector

The ATLAS detector comprises of the inner detector (ID), the magnetic system, the Electromagnetic (EM) calorimeter, the Hadronic calorimeter and the Muon spectrometer. The ID tracks charged particles and is surrounded by a 2 T superconducting solenoid which bends the particles to enable particle momentum measurements, particle identification and vertex measurements. The ID covers a pseudorapidity range of  $|\eta| < 2.5$  [9]. The EM calorimeter surrounds the ID and absorbs energy from particles which interact electromagnetically. The EM calorimeter covers  $|\eta| < 3.2$ . Surrounding it is the Hadronic calorimeter which is also a sampling calorimeter made up of steel plates and plastic scintillator plates which absorb energy from hadrons. These provide a hadronic coverage of  $|\eta| < 1.7$  and LAr technology is also used for the hadronic calorimeter end-cap region. The outermost part of the detector is made up of the muon spectrometer which consists of three large superconducting toroid systems which provide exceptional muon momentum measurements through accurate tracking.

## 3. Object selection

Events are required to have at least two photon candidates with  $p_T > 25$  GeV and within  $|\eta| < 2.3$ . A ‘tight’ photon identification requirement is applied to the candidates in order to reduce misidentification [10]. Isolation variables are also applied to further reject hadronic backgrounds. The photons are required to have  $p_T/m_{\gamma\gamma} > 0.35$  and 0.25, respectively. Events are required to have  $105 \text{ GeV} < m_{\gamma\gamma} < 160 \text{ GeV}$  where the diphoton mass is calculated assuming that the photons originate from the diphoton primary vertex. Jets are reconstructed from energy clusters in EM and hadronic calorimeters using the anti-kt algorithm. They are required to have  $p_T > 20$  GeV and be within  $|\eta| < 4.5$ . The jets with  $|\eta| < 2.4$  and  $p_T < 60$  GeV must pass the jet vertex tagger selection. Electrons are reconstructed from energy clusters in the EM calorimeter, associated with tracks reconstructed in the ID. Electrons with  $p_T > 10$  GeV and  $|\eta| < 2.47$  are selected. Muons are reconstructed from tracks in the inner detector and the muon spectrometer. Those with  $p_T > 10$  GeV and  $|\eta| < 2.7$  are selected and in the region  $|\eta| < 2.5$ , they must be matched to ID tracks.

Missing transverse energy is described as the energy which is not detected in a particle detector but is expected due to the laws of conservation of energy and momentum. At the LHC, the initial energy of the particles which travel transverse to the beam axis is zero thus any net momentum in the transverse direction is an indication of  $E_T^{\text{miss}}$ . This vector momentum imbalance in the transverse plane is obtained from the negative vector sum of the momenta of all particles detected.  $E_T^{\text{miss}}$  of the track based soft term (TST) is used in this analysis. The selected photons, jets and leptons are injected into the  $E_T^{\text{miss}}$  calculation. Both the soft term and the jets are reconstructed with respect to the photon pointing vertex. In 2016 the large increase of additional proton-proton collisions lead to the degradation of the performance of the  $E_T^{\text{miss}}$ . In order to alleviate this problem the variable  $S_{E_T^{\text{miss}}} = E_T^{\text{miss}}/\sqrt{\sum E_T}$  was introduced. The actual value of  $E_T^{\text{miss}}$  is calculated as follows [9]:

$$E_T^{\text{miss}} = \sqrt{(E_x^{\text{miss}})^2 + (E_y^{\text{miss}})^2} \quad (1)$$

#### 4. Categorization

This analysis defines five sequential categories shown in table 1. In the heavy-scalar model, the spectra of  $E_T^{\text{miss}}$  and  $p_{yy}^T$  are shifted to smaller values. The same vertex selection occurs when the distance between the diphoton vertex and the highest  $\sum p_T^2$  vertex in the z direction is less than 0.1 mm.

**Table 1:** Set categories defined sequentially in the rows and each category excludes events in the previous row.

<i>Category</i>	<i>Requirements</i>
Mono-Higgs	$S_{E_T^{\text{miss}}} > 7 \sqrt{\text{GeV}}, p_T^{\gamma\gamma} > 90 \text{ GeV}$ , lepton veto
High- $E_T^{\text{miss}}$	$S_{E_T^{\text{miss}}} > 5.5 \sqrt{\text{GeV}},  z_{\text{PV}}^{\text{highest}} - z_{\text{PV}}^{\gamma\gamma}  < 0.1 \text{ mm}$
Intermediate- $E_T^{\text{miss}}$	$S_{E_T^{\text{miss}}} > 4 \sqrt{\text{GeV}}, p_T^{\text{hard}} > 40 \text{ GeV},  z_{\text{PV}}^{\text{highest}} - z_{\text{PV}}^{\gamma\gamma}  < 0.1 \text{ mm}$
Different vertex	$S_{E_T^{\text{miss}}} > 4 \sqrt{\text{GeV}}, p_T^{\text{hard}} > 40 \text{ GeV},  z_{\text{PV}}^{\text{highest}} - z_{\text{PV}}^{\gamma\gamma}  > 0.1 \text{ mm}$
Rest	$p_T^{\gamma\gamma} > 15 \text{ GeV}$

For the control distributions shown in figure 2, the normalizations of the  $\gamma\gamma$  and  $\gamma$ +jet contributions are fixed to 79% and 19% of the data yield, estimated from a two-dimensional sideband technique which involves counting the number of events in which one or both photons pass or fail the identification or isolation requirements [11]. Slight discrepancies are observed in the control distributions above, but these do not affect the overall results. The inconsistencies are found mainly in non-resonant backgrounds, which are estimated directly from data.

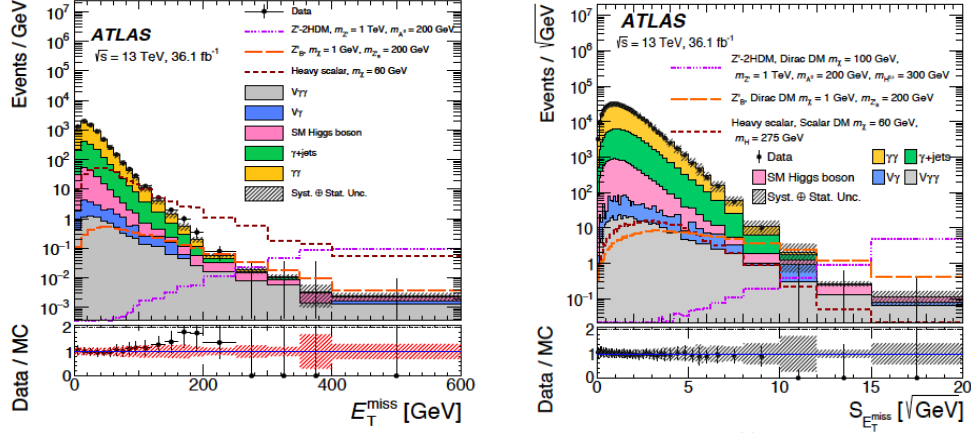


**Figure 2:**  $E_T^{\text{miss}}$  and  $S_{E_T^{\text{miss}}}$  distributions after the selection of diphoton candidates within  $105 \text{ GeV} < m_{\gamma\gamma} < 160 \text{ GeV}$ . The heavy-scalar signal corresponds to  $m_H = 275 \text{ GeV}$  and scalar DM  $m_\chi = 60 \text{ GeV}$ .

## 5. Systematic Uncertainties

The systematic uncertainties from experimental and theoretical sources affect the signal efficiency and the SM Higgs background yield estimated from simulated MC samples. A summary of the experimental and theoretical uncertainties with respect to the yield of the background is shown in table 2.

**Table 2:** Breakdown of the dominant systematic uncertainties in the range of  $105 \text{ GeV} < m_{\gamma\gamma} < 160 \text{ GeV}$ .

<i>Source</i>	<i>Signals</i> [%]	<i>Backgrounds</i> [%]
Experimental		
Luminosity	3.2	-
Trigger efficiency	0.4	-
Vertex selection	< 0.1	-
Photon energy scale	0.1-2.0	0.1-1.4
Photon energy resolution	0.1-0.2	0.1-1.1
Photon identification efficiency	2.9-4.3	1.9-3.8
Photon isolation efficiency	1.2	0.8-1.6
$E_T^{\text{miss}}$ reconstruction (diphoton vertex)	< 0.1	0.5-1.9
$E_T^{\text{miss}}$ reconstruction (jets, soft term)	1.0-1.4	0.8-23
Diphoton vertex with largest $\sum p_T^2$	< 0.1-1.9	0.1-6.0
Pileup reweighting	0.2-5.6	0.7-11
Non-resonant background modelling	-	0.1-9.8
Theoretical		
Factorization and renormalization scale	0.6-11	2.5-6.0
PDF+ $\alpha_s$	11-25	1.2-2.9
Multiple parton-parton interactions	< 1	0.4-5.8
$B(H \rightarrow \gamma\gamma)$	1.73	-

Values for the impact on all categories are shown and in the cases where the value is substituted by a “–”, the systematic uncertainty is not applicable to the sample. If a given source has a different impact on the various categories, the given range corresponds to the smallest and largest impacts. The most important uncertainties in this analysis are those in jet energy scale, resolution and jet vertex tagger which are propagated to the  $E_T^{\text{miss}}$  calculation. These need to be taken into account in order to avoid misreconstruction of  $E_T^{\text{miss}}$ , which can lead to the migration of events among categories.

## 6. Results

Results for the analysis are derived from a likelihood fit of the  $m_{\gamma\gamma}$  distribution in the range  $105 \text{ GeV} < m_{\gamma\gamma} < 160 \text{ GeV}$ . Figure 3 shows the  $m_{\gamma\gamma}$  distributions in the five categories as well as the fitted contribution of a heavy-scalar boson for illustration.

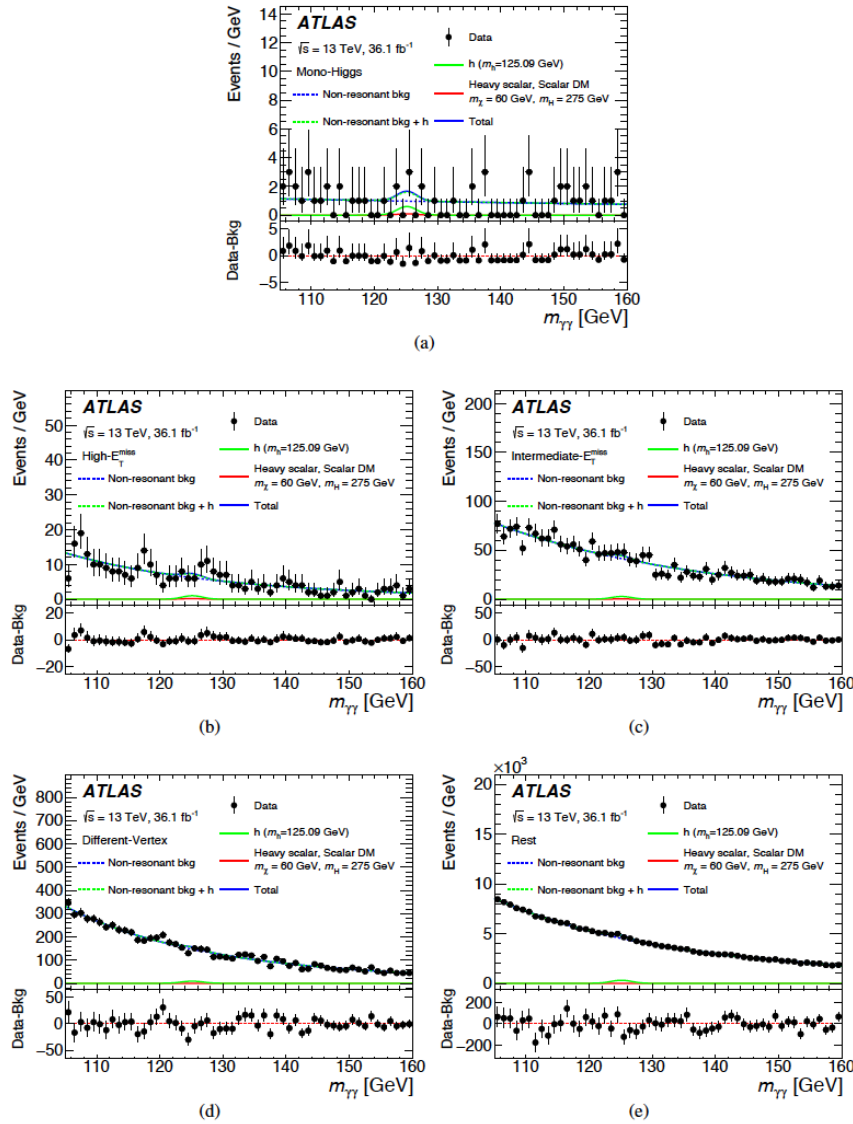


**Figure 3:** Diphoton invariant mass distribution for data and the corresponding fitted signal and background in the five categories. No significant excess of events is observed in any category.

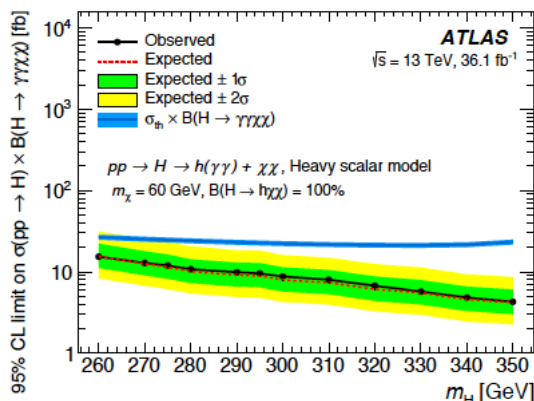


**Figure 4:** Observed and expected 95% CL upper limits on the  $\sigma(pp \rightarrow H) \times B(H \rightarrow \gamma\gamma\chi\chi)$  as a function of  $m_H$  for  $m_\chi = 60$  GeV as a function of the heavy-scalar-boson mass in the range  $260 \text{ GeV} < m_H < 350 \text{ GeV}$ .

The 95% CL upper limits on the  $\sigma(pp \rightarrow H) \times B(H \rightarrow \gamma\gamma\chi\chi)$  as a function of  $m_H$  for  $m_\chi = 60$  GeV is shown in figure 4. A 100% branching fraction is assumed for  $H \rightarrow h\chi\chi$ . No significant excess is observed.

## 7. Conclusions

A search for new physics in association with  $E_T^{\text{miss}}$  and a Higgs boson decaying to two photons in association with  $E_T^{\text{miss}}$  has been presented [6]. This study is based on data corresponding to an integrated luminosity of  $36.1 \text{ fb}^{-1}$  of p-p collisions at the LHC at a center-of-mass energy of 13 TeV. In Run II of data taking, an improved  $E_T^{\text{miss}}$  definition has been implemented. Good  $E_T^{\text{miss}}$  reconstruction is fundamental in BSM searches. For this analysis 95% CL upper limits were set on the production cross section times the branching fraction of  $H \rightarrow h\chi\chi \rightarrow \gamma\gamma\chi\chi$ , where a 100% branching fraction is assumed for  $H \rightarrow h\chi\chi$ . No significant excess over the expected background is observed. However, the benchmark point assumes 100% branching ratio, which is an extreme case, thus we have to look at other decay channels to observe possible excesses. This does not mean we are excluding the heavy-scalar model, rather we are understanding the nature of  $H$  better. It would be useful to explore cases where the branching ratio is not 100% with more data.

## References

- [1] ATLAS Collaboration 2012 *Physics Letters B* **716** 1–29 ISSN 03702693 (*Preprint* 1207.7214)
- [2] CMS Collaboration 2012 *Physics Letters B* **716** 30–61 ISSN 03702693 (*Preprint* 1207.7235)
- [3] Bertone G, Hooper D and Silk J 2005 *Phys. Rept.* **405** 279–390 (*Preprint* hep-ph/0404175)
- [4] Sirunyan A M *et al.* (CMS) 2017 (*Preprint* 1703.05236)
- [5] Aad G *et al.* (ATLAS) 2016 *Phys. Rev.* **D93** 072007 (*Preprint* 1510.06218)
- [6] Aaboud M *et al.* (ATLAS) 2017 (*Preprint* 1706.03948)
- [7] Abercrombie D *et al.* 2015 (*Preprint* 1507.00966)
- [8] von Buddenbrock S, Chakrabarty N, Cornell A S, Kar D, Kumar M, Mandal T, Mellado B, Mukhopadhyaya B, Reed R G and Ruan X 2016 *Eur. Phys. J.* **C76** 580 (*Preprint* 1606.01674)
- [9] ATLAS Collaboration 2012 *The European Physical Journal C* **72** 1844 ISSN 1434-6044 (*Preprint* 1108.5602)
- [10] Aaboud M *et al.* (ATLAS) 2016 *Eur. Phys. J.* **C76** 666 (*Preprint* 1606.01813)
- [11] Aad G *et al.* (ATLAS) 2013 *JHEP* **01** 086 (*Preprint* 1211.1913)